Case Studies in Thermal Engineering 68 (2025) 105925

Contents lists available at ScienceDirect

Case Studies in Thermal Engineering

journal homepage: www.elsevier.com/locate/csite

An experimental study on the effect of lobe swirl device and its transition parts on thermal performance using Graphene-CuO/water nanohybrid

Farag A. Diabis [a], Abd Rahim Abu Talib [a,b,c,*], Norkhairunnisa Mazlan [a,b], Eris Elianddy Supeni [d]

[a] Aerodynamic, Heat Transfer and Propulsion Group, Department of Aerospace Engineering, Faculty of Engineering, Universiti Putra Malaysia, Serdang, 43400, Selangor, Malaysia
[b] Aerospace Malaysia Research Centre, Faculty of Engineering, Universiti Putra Malaysia, Serdang, 43400, Selangor, Malaysia
[c] Universiti Kuala Lumpur Malaysian Institute of Aviation Technology (UniKL MIAT), Lot 2891 Jalan Jenderam Hulu, 43800, Dengkil, Selangor, Malaysia
[d] Department of Mechanical and Manufacturing Engineering, Faculty of Engineering, Universiti Putra Malaysia, Serdang, 43400, Selangor, Malaysia

HIGHLIGHTS

- *The impact of a lobed swirl generator over a circular tube on heat transfer and friction factor is discussed.*
- *The effect of a lobed swirl generator using GO-CuO/water nanohybrid on thermal performance is also investigated.*
- *The outcome demonstrated that the lobed swirl generator remarkably affects thermal performance improvement.*

ARTICLE INFO

Keywords:
Lobed swirl device
Transition parts
GO-CuO/water nanohybrid
Nusselt number
Friction factor

ABSTRACT

Enhancing heat transfer efficiency is a key focus in thermal applications. Smooth channels often suffer from poor fluid mixing, limiting their performance. Swirl flow techniques have been introduced to improve heat exchanger efficiency by altering flow direction and inducing turbulence. However, integrating nanofluids with swirl techniques presents challenges such as increased pressure loss and nanoparticle sedimentation. The four-lobed swirl generator is a promising solution, delivering high swirl intensity with manageable pressure loss. This study explores the impact of GO-CuO/water hybrid nanofluid and Reynolds numbers on the thermal performance of a four-lobed swirl generator. The system parameters include a twisted angle ($\theta = 360^\circ$), β-transition type, transition multiplier (n = 0.5 mm), and a variable helix (t = 1). The hybrid nanofluid, synthesized with a 20 % GO to 80 % CuO ratio, has volume concentrations of 0.15%–0.75 % wt., with Reynolds numbers from 15,000 to 35,000. Results indicate a significant heat transfer enhancement (1.26–1.72 times) with a moderate friction factor increase (1.27–1.53). The highest thermal performance (1.511) occurs at 0.75 % nanofluid concentration and $Re = 25{,}000$. This study confirms the four-lobed swirl generator's effectiveness in improving heat exchanger efficiency while maintaining an acceptable pressure drop.

* Corresponding author. Aerodynamic, Heat Transfer and Propulsion Group, Department of Aerospace Engineering, Faculty of Engineering, Universiti Putra Malaysia, Serdang, 43400, Selangor, Malaysia.
E-mail address: abdrahim@upm.edu.my (A.R. Abu Talib).

https://doi.org/10.1016/j.csite.2025.105925
Received 25 October 2024; Received in revised form 13 February 2025; Accepted 18 February 2025
Available online 19 February 2025

Nomenclature

A	area (m^2)	α	alpha transition
$\dot{m}$	mass flow rate (kg/s)	n	transition multiplier (mm)
h	heat transfer coefficient (W/m^2. K)	L_t	length of transition (mm)
Q	heat transfer (W)	$f\&f_1$	variables to facilitate y calculation
Nu	Nusselt number	y	variable length from transition core origin (mm)
Pr	Prandtl number (μ.Cp/k)	*Creek letter*	
K	thermal conductivity (W/m. K)		
Re	Reynolds number ($=u_{in}D/\nu$)	ρ	density (kg/m^3)
ΔP	pressure drop (Pa)	μ	viscosity (Pa.s)
ΔT	temperature different (K)	φ	solid volume concentration (%)
L	test section length (m)	θ	twisted angle (degree)
u	velocity (m/s)	*Sup/Superscripts*	
f	friction factor		
R	test section radius (m)	s	surface
T	temperature (K)	p	plane tube
Cp	Specific heat (J.kg/K)	ave	average
Lobed swirl notation		in	inlet
		cs	circle inscribe
A_{4L}	area of four segments (mm^2)	FD	fully developed
r_{lobe}	lobe swirl radius (mm)	i	intermediate
R_{cs}	swirl core radius (mm)	Abbreviations	
LA_i	intermediate area (mm^2)	PEC	Performance Evaluation Criteria
LA_{FD}	fully developed area (mm^2)	DSC	Differential Scanning Calorimetry
β	beta transition	SEM	Scanning Electron Microscope

1. Introduction

Technologies and thermal science advancements have led to severe challenges in energy imbalance. This predicament required the development of novel cooling systems capable of meeting industrial demands and improving thermoregulation effectiveness [1]. In recent years, various alternative techniques have been explored to enhance the thermal performance of heat exchangers, particularly in power plant applications. [2], chemical engineering [3], the cooling system in different areas [4], waste heat recovery [5] etc. According to several studies, over 60 % of the energy consumed across various industries is lost as waste heat. Consequently, the development of efficient waste heat recovery technologies has become imperative to enhance both energy sustainability and environmental security [6]. Flow separation is vital in designing various technical applications that need heating or cooling [7]. Nowadays, the trend for higher speeds in many innovations has resulted in excessive heating. Consequently, cooling them down has become a significant challenge for many researchers [8].

The mechanism of applying helical pipe in the field of heat transfer is represented in (i) the characteristics of its curvature geometry, which results in inducing the velocity and secondary flow, and (ii) creating the mixing flow between the core and the wall [9]. The features of the swirling flow of intensive secondary flow, a reduction in the thermal boundary layer, and mixing fluid close to the wall play the leading role in promoting a higher heat transfer rate over single-phase as multiphase flows [10]. One of the three well-known methods listed below can be used to generate the swirling flow: (i) fluid flow attains tangential velocity and enters the pipe as a swirl flow after passing through a rotating segment, (ii) enabling the fluid flow to enter the pipe via fixed blades (vanes) placed within the pipe at a certain angle, and (iii) the working fluid enters the pipe as a tangential inlet to gain rotational velocity and enter the pipe as a swirling flow [11]. Extended surfaces are widely employed as a thermal management strategy for heat transfer enhancement due to their capability to increase the effective surface area, thereby improving overall heat dissipation [12]. The impact of three types of ribbed tubes on heat transfer using TiO_2 nanofluid as a working fluid has been conducted by AlKumait et al., [13]. The configurations of longitudinal, helical, and circumferential tubes were analyzed under varying pitch distances of 5.89 mm, 7.86 mm, and 11.79 mm. Among all the investigated tube designs, the helical tube exhibited the highest turbulent kinetic energy, achieving a performance evaluation criterion (PEC) of 2.0 % at a pitch distance of 5.89 mm. The result demonstrated that the helical shape induces a swirling motion in the fluid, which increases the fluid's turbulence. This swirl can enhance both mixing and heat transfer by disrupting the boundary layer near the tube surface and improving the overall contact between the fluid and the surface. The quantity of heat transfer in any system or process can be evaluated through thermodynamic analysis. In thermodynamic studies, heat transfer is examined concerning a system undergoing a transition from one equilibrium state to another. This process requires a heat-transferring device, known as a heat exchanger, which effectively dissipates heat from the heat source to a region with a lower temperature [14]. A comparison between the impact of perforated fins and non-perforated on thermal-hydraulic characteristics has been conducted by Ibrahim et al. [15]. In general, the result proved that the augmentation of perforation numbers led to a higher heat transfer rate. It can be explained by the increase in turbulence flow level and reduce the thermal resistance.

The lobed swirl generator is one of the recent innovations that faced the energy crisis. The advantage of a lobed swirl generator is represented in its ability to produce tangential velocity adjacent to the wall, axial velocity noticeable at the core, and reduce pressure losses [16]. Recently, many researchers have addressed the effect of swirl generators with pure working fluid on heat transfer improvement [17]. Jafari et al. [18] studied numerically and experimentally the impact of the three-lobe swirl generator on the fluid flow field and heat transfer enhancement. The author also examined the effect of four-lobe [10] and five-lobed [19]. Among all lobed swirl generators investigated, a four-lobe swirl generator at the angle of 360° and the length of 400 mm presented the highest heat transfer enhancement at Nusselt number (*Nu*) of the range from 1.4 to 1.9 and thermal performance from 1.30 to 1.65 with an acceptance of pressure drop from 1.22 to 1.48. Diabis et al. [20] considered the effect of a four-lobed swirl generator and its transition part on thermal performance enhancement numerically using different types of nanofluid. Using SiO_2 at a *Re* of 15,000, the study showed the most significant improvement in thermal performance by a factor of 1.67. The effect of tri-lobe and twisted oval tubes on thermal performance and fluid flow field was experimentally and numerically investigated by Tang et al. [9]. The study was performed at different cross-sections, lobed numbers and different directions twisted. The study revealed that the tri-lobed promotes heat transfer enhancement at 5.4 % more than the oval tube. The effect of short twisted oval and three-lobed twisted tubes on the improvement of heat transfer and pressure drop was explored by Indurain et al. [21]. The study demonstrated that the twisted three-lobe ST3L produces greater swirl intensity than the oval tube, especially at an aspect ratio of $c = 0.6$ with a noticeable increase in pressure drop. The author recommended a short-twisted length to address the pressure drop penalty. The effect of a three-lobe swirl generator combined with a Y-tape insert on heat transfer promoting and turbulent flow characteristics was numerically investigated by Omidi et al. [22]. The study employed a working fluid of pure water and Al_2O_3-water nanofluid at different volume concentrations from (1 %–3 % wt.). The study proved that the Y-tape technique combined with a twisted tube led to increased heat transfer and decreased thermal performance due to the dramatic increase in pressure drop. Therefore, adding nanoparticles to the lobe swirl generator is more practical with an empty tube.

Omidi and Farhadi [16] investigated the effect of the double pipe heat exchanger at different inner and outer geometrical cross-sections and lobe numbers on thermal performance and fluid flow characteristics. Among all cases, the study identified the 3-lobe inner and outer cross-sections as the most beneficial configuration, demonstrating a 3.13-fold improvement in thermal performance. The impact of the lobe swirl generator under different lobes number (*n*) and pitch to diameter (*P:D*) on the characteristics of the fluid flow field was carried out by Yan et al. [23]. The study confirmed that a four-lobed swirl generator associated with a pitch-to-diameter (8) provided the highest swirl effectiveness with an applicable pressure drop. Li et al. [24] investigated the effect of the four-lobe swirl generator at the fixed transition length of 100 mm and different swirl device lengths at 200 mm and 400 mm on tangential velocity, pressure drop and overall swirl effectiveness. The study confirmed that the short four-lobe swirl generator of 100 + 200+100 presented more incredible tangential velocity and less pressure drop leading to inducing better swirl effectiveness than the lobe swirl of 100 + 400+100. The unique transition part of swirl-inducing pipes has been designed with remarkable beneficial impact by Ariyaratne and Jones [25]. Based on the observed lobe growth along the tube, an optimized entrance and exit transition shape was developed. The study demonstrated that these transition sections contributed to a reduction in pressure losses. Additionally, the entry transition enhanced swirl intensity, while the exit transition mitigated swirl decay, thereby improving overall flow dynamics.

The dispersion of two or more types of nanoparticles within a base fluid is referred to as a hybrid nanofluid. Due to their significantly larger relative surface area compared to the base fluid, hybrid nanoparticles enhance key transport properties, including

Table 1
Previous studies of Graphene oxide characteristics after its incorporation with several types of oxide nanoparticles under different effective parameters.

Ref.	Hybrid Nanomaterial volume ratio	Base fluid	Nanoparticles Diameter (nm)	Volume fraction percentage (%)	Temperature range (°C)	Maximum Thermal conductivity improvement
[32]	GO/CuO (50:50) & (20:80)	Water	GO (N-A) CuO (13)	0.1 to 1 wt%	30-60 °C	GO/CuO (50:50) presented 41 %, at 60 °C for 1 vol%,
[33]	GO/Al_2O_3(50:50)	Water	GO (3.3–7), AL_2O_3 (20)	0.1 to 1 wt%	25-50 °C	33.9 % at 1 vol % & 50 °C
[34]	GO/CuO (50:50)	Water-EG (50:50)	GO (3.3–7), CuO (40)	0 to 1.6 wt%	25-50 °C	43.4 % at 1.6 vol%
[35]	RM/GO (50:50)	Water	RM (29), GO (21.5)	0.1–0.75 vol%		
[36]	GO/TiO_2	Water	GO (3.3–7), TiO_2 (20)	0.05 to 1 wt%	20-50 °C	32.8 % at 1 vol1 % 50 °C
[37]	GO/CuO (20:80)	Distilled water	GO (1–4), CuO (20)	0.03, 0.1 & 0.2 wt%	30 °C, 45 °C & 60 °C	30 % at vol.0.3 % & 60 °C
[38]	GO/MgO	Water-EG (80:20)	GO (3.3–7), MgO (20)	0.025 to 0.2 wt%	20-60 °C	8.8 % at vol.0.2 %
[39]	Al_2O_3/GO (50:50) & Al_2O_3/GO (80:20)	Water	Al2O3 (30) GO (N-A)	0.1 to 0.5 wt%	30-60 °C	Al_2O_3/GO (50:50) presented 32.1 %, at 60 °C for 0.5 vol%,
[40]	SiO2/Graphene (70:30)	Water	SiO_2 (50), GO (28.21–40.79)	0.05 to 1 wt%	25-50 °C	36.12 % at vol.1 %
[41]	GO/Ag	EG	SiO_2 (50) GO (−), Ag (4–7)	0.1 to 0.3 wt%	20-50 °C	22 % at vol.0.3 % & 45 °C
[42]	TiO_2-graphene	Water	TiO_2 (10–25), Graphene (2–18)	0.005 to 0.5 wt%	25 to 75 °C	27.84 % at vol.0.5 % & 75 °C
[43]	GO/Al_2O_3 (50:50) & (20:80)	Water	Al_2O_3 (30) GO (N-A)	0.1 to 1 wt%	30-60 °C	GO NF is 5.8, 12.8 and 43.9 % greater than GO/Al_2O_3 (50:50), GO/Al_2O_3 (20:80) and Al_2O_3 NFs at 60 °C for a concentration of 1 vol%,
[44]	GO/Al_2O_3	water- EG	N-A	0.1 to 1.6 wt%	20 °C to 55 °C	20 % at vol.1.6 % & 55 °C
[45]	Cu/GO (30:70 & 70:30)	Water	GO (<2), Cu (30–50)	0.01 % and 0.02. wt.%	Room Temperature	32.31 % at vol. 0.02 % & 30:70 (GO/Cu)

thermal conductivity and heat transfer coefficient. This improvement makes hybrid nanofluids highly attractive for various thermal applications [26]. Many studies have revealed that hybrid nanoparticles play a vital step in terms of thermal performance improvement. Hybrid nanofluids have been shown to exhibit superior thermophysical properties compared to mono nanofluids [27]. Brownian motion appears to be more pronounced in hybrid nanofluids compared to mono nanofluids [28]. The concept of constructing thermal bridges to minimize heat flow resistance is indeed an interesting approach, especially in the context of hybrid nanofluids [28]. The main goal of dispersing nanoparticles into a base fluid is to significantly enhance the heat transfer properties of the fluid, making it more efficient for applications in thermal management systems. This idea is foundational to the development of nanofluids and hybrid nanofluids, where the combination of base fluids and nanoparticles creates a material with superior thermal conductivity, viscosity, and other thermo-physical properties compared to the base fluid alone [29]. Hybrid nanofluids indeed represent an advanced and more efficient class of thermal fluids compared to mono-nanofluids. By dispersing two or more different types of nanoparticles into a base fluid, hybrid nanofluids can provide significantly enhanced thermophysical properties, such as thermal conductivity, stability, and overall performance. This dual-particle approach leverages the distinct properties of each type of nanoparticle to improve the overall characteristics of the fluid [30]. One of the main reasons for adopting hybrid nanofluids is to achieve enhanced thermal conductivity while maintaining a balance between cost-effectiveness and stability [31]. Table 1 summarises the results of incorporating graphene oxide (GO) with various nanomaterials under different parameters.

It can be concluded that the GO/CuO presented the highest thermal conductivity among all hybrid nanofluids investigated by different researchers. Studies indicate that graphene nanoparticles offer several benefits, including increased stability, less corrosion, a larger surface area to volume ratio, decreased erosion and clogging, a diminished requirement for pumping power, increased thermal conductivity, and notable energy savings [46]. According to copper oxide, not only can CuO nanofluids have a high thermal conductivity, it is also have good compatibility with basic liquids and are reasonably priced [47]. Therefore, GO/CuO hybrid nanofluid has been adopted in the current study.

From the literature review and other comprehensive studies, it can be proved that applying a lobe swirl generator in the field of thermal application can improve thermal performance with a practical level of pressure loss. Despite extensive research on swirl flow techniques and nanofluid applications in heat transfer enhancement, insufficient attention has been given to the thermal performance of lobed swirl generators in conjunction with GO-CuO/water hybrid nanofluids. Furthermore, while graphene oxide (GO) and copper oxide (CuO) nanofluids have been individually explored for their thermal properties, their combined effect in a hybrid nanofluid, particularly within a lobed swirl flow environment, still needs to be examined. This research, therefore, addresses a critical knowledge gap by experimentally investigating the effects of a four-lobed swirl generator and GO-CuO/water hybrid nanofluids on heat transfer, pressure loss, and overall thermal performance.

Also, the interplay between heat transfer enhancement and pressure loss in advanced swirl generators has yet to be comprehensively analyzed under varying Reynolds numbers. The most significant recent development is the lobed swirl generator, which produces considerable swirl intensity with an applicable pressure loss. Therefore, the motivation behind this study is to investigate and acquire a deeper understanding of the lobed swirl generator's thermal characteristics under various effective parameters. The study also aims to address a unique research gap by leveraging the significant advantages of lobed swirl generators, as highlighted in the literature, particularly their ability to maintain particle suspensions due to the inclusion of specialized entry and exit transition parts. While swirl flow techniques have demonstrated their effectiveness in heat transfer enhancement, the optimization of lobed swirl

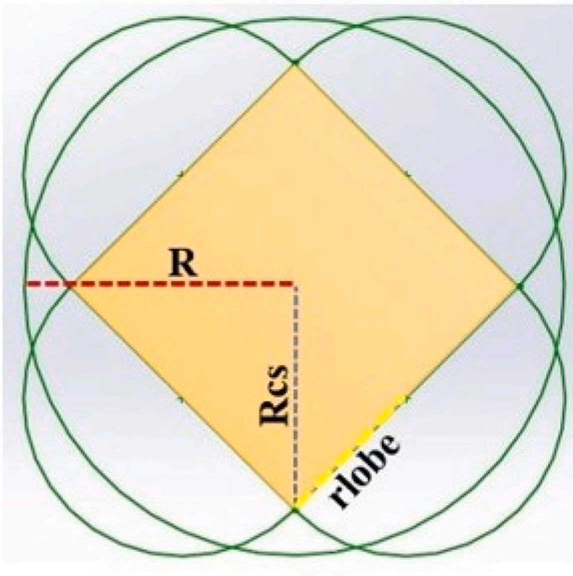

Fig. 1. Main radii in lobe swirl device (r_{lobe} and R_{cs}).

generators in combination with nanofluids remains an area requiring further exploration. Limited studies have investigated the impact of GO-CuO/water hybrid nanofluid in conjunction with lobed swirl generators, particularly under varying operating conditions. Understanding how different geometrical parameters, nanofluid compositions, and Reynolds numbers influence thermal performance is crucial to advancing the applicability of these techniques in real-world heat exchange systems. This study aims to fill this gap by experimentally analysing the thermal properties of a four-lobed swirl generator under different effectiveness parameters. Therefore, the objective of the current study is to investigate experimentally the thermal performance of a lobed swirl generator at its optimal parameters such as four-lobed number, twisted angle of $\theta = 360^\circ$, β-transition type, transition multiplier of $n = 0.5$ mm, and variable helix of $t = 1$ mm. To determine and understand the thermal characteristics and the mechanism of lobed swirl generators under hybrid nanofluid of 20 % GO to 80 % CuO/water as a working fluid at different volume concentrations (0.15 %–0.75 % wt.) for different Reynolds numbers in The range of 15,000 to 35,000.

2. Model in physical form

2.1. Four-lobe swirl device

Swirl flow is characterized as a mixture of a vortex and axial movements with spiral streamlines [48]. The present study adopted the Reference Geometry Plane method and Left Boss/Base feature using Solidworks software to obtain the geometrical cross-section. According to the literature review, a lobe swirl device at 200 mm length and an equivalent diameter of 0.5 m were proved to be effective parameters. During the creation of the swirl device, key parameters such as the lobe radius (r_{lobe}), polygonal cross-sectional radius (R_{cs}), tube radius (R), and twist angle (θ) are considered. Fig. 1 depicts the primary radii adopted to evaluate the four-lobe swirl device.

As shown in Fig. 2(a), 21 planes were divided and allocated parallel to create the lobe swirl device. The distance between every two adjacent at 10 mm ($x/L = 0.05$) to avoid the steeper and ensure the constant twisted angle over the geometrical cross-section is also taken into account. Therefore, based on the suggested swirl angle of (360°), each adjacent plane would have a slope of 18° [49]. Several studies proved that the remarkable effectiveness of a four-lobe swirl generator could be obtained under an equivalent diameter of 0.5 m and pitch to a diameter of $P{:}D = 8$ [50]. Therefore, the values of the lobed swirl radius at $r_{lobe} = 13.81$ mm and the lobed swirl core radius at $R_{cs} = 19.54$ mm as a fully developed cross-section using Eqs. (1) and (2) were evaluated [23]. As shown in Fig. 2(b), the swirl device at 3 mm in thickness and ABS material was manufactured by a plus 3D printer using Cubicreator software.

$$r_{lobe} = \sqrt{\frac{2\pi \tan\left(\frac{360}{8}\right) R^2}{8 + 4\pi \tan\left(\frac{360}{8}\right)}} \tag{1}$$

$$R_{CS} = \frac{r_{lobe}}{\sin\left(\frac{360}{8}\right)} \tag{2}$$

The cross-sectional area, the perimeter and the hydraulic diameter are evaluated using Eqs. (3)–(5) as follows: The four lobes area (A_{4L}) = the polygon area at the centre (A_p) + the area of four segments on the sides (A_{4s}) [10,23]. Therefore,

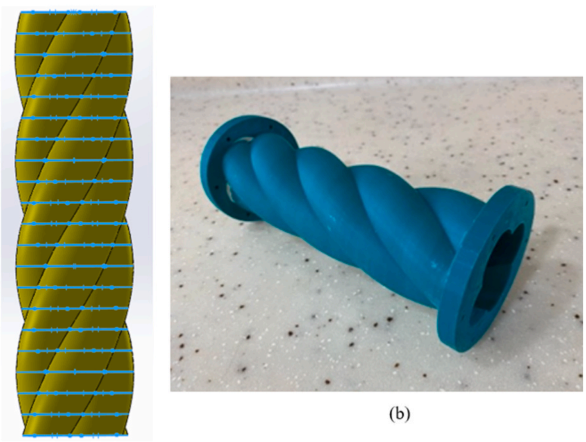

(a) (b)

Fig. 2. (a) Development of lobed swirl device under 21 planes, (b) Lobe swirl device manufactured.

$$A_{4L} = \frac{r_{lobe}^2}{\tan\left(\frac{360}{2n}\right)} \times n + \frac{\pi r_{lobe}^2}{2} \times n \tag{3}$$

$$P_{4L} = n \times \frac{2\pi r_{lobe}}{2} \tag{4}$$

$$D_{h_{4L}} = \frac{4A_{4L}}{P_{4L}} \tag{5}$$

2.2. Transition parts

The transition section is considered an indispensable parameter to increase the efficacy of the lobed swirl intensity and reduce the pressure losses of swirl flow downstream [51]. To the best of our knowledge and based on past studies, a sudden change in geometry during fluid flow causes an increase in pressure losses [25]. Therefore, it is noticeable that the development of the transition part progressively from a circular cross-section to a lobe shape and vice versa led to a reduction in pressure drop as well as a significant increase in the effectiveness of the lobed swirl. As a result, the transition part cross-section was created using SolidWorks 2015 software, with the reference geometry plane and lofted boss/base features. Based on the twisted degree, which was calculated using Eq. (6), the length of the transition part was determined using Eq. (7). The transition part was turned quarter (1/4) or an angle of (90°) to ensure the gradual change of the geometrical cross-section and avoid an augmentation in pressure losses [25]. Two essential variables ($f \& f_1$) based on trigonometric function have been introduced using Eqs. (8) and (9) to facilitate (R & y) calculation. During the development of the transition part from one stage to another, the core radius (R) was evaluated using Eq. (10). As implied in Eq. (11), the variable (y) was used to keep the cross-section of the lobe area equal at each step. After implementing all the parameters mentioned above, the area at the intermediate (LA_i) and fully developed stage (LA_{FD}) becomes accessible to calculate using Eqs. (12) and (13).

The cosine function has been applied using Eq. (14) to avoid discontinuity development during the expansion of the transition part, particularly at the start and end regions [51]. To specify the twisting and its direction at the intermediate region, Eq. (15) is utilized. To control the area development along the transition pipe, two essential variables known as the Beta transition (α) and Alpha transition (β) should be considered. Ariyaratne & Jones [25] revealed that the Beta transition (β) was more effective in swirl induction than the Alpha transition, with a swirl productivity value of 5 % higher. Therefore, the Beta transition (β) was adopted in the current experimental study. Therefore, Eq. (16) was used to evaluate the Beta transition at the transition multiplier (n = 0.5 mm), which was also introduced by Ariyaratne & Jones [25] as an essential factor that directly affected the curvature of the transition part in each stage. The lobed swirl transition part from different sides and under 18 planes is illustrated clearly in Fig. 3(a). Finally, the transition parts have been fabricated at 3 mm of thickness using ABS material, as shown in Fig. 3(b). All the equations used to create transition parts are evaluated [49] as follows:

$$twist\ (degree\,/\,m) = \frac{360}{(P : D_{ratio}) \times de} \tag{6}$$

Where *P:D* refers to pitch to diameter while *de* refers to hydraulic diameter

$$L_t = \frac{1000mm}{Twisted(degree/m)} \times 90^\circ \tag{7}$$

$$f = \left(\gamma - \frac{1}{2} \sin 2\,\gamma\right) \tag{8}$$

$$f_1 = \frac{1}{\sqrt{2}}\left[1 - \frac{1}{\tan\gamma}\right] \tag{9}$$

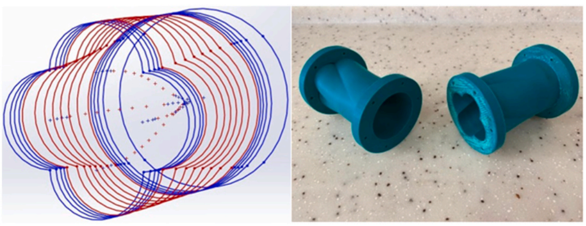

(a) (b)

Fig. 3. (a) Transition part with 17 planes, (b) transition parts fabricated.

$$R = R_1 \sqrt{\frac{\pi}{4f + 4ff_1^2 - 4\sqrt{2}ff_1 + 2}} \tag{10}$$

$$y = f_1 \times R \tag{11}$$

$$LA_i = 4fr_{lobe}^2 - R^2(\pi - 2) \tag{12}$$

$$LA_{FD} = r_{lobe}^2(4 + 2\pi) - \pi R_{CS}^2 \tag{13}$$

$$\frac{X}{L} = \cos^{-1}\left(\frac{1 - 2(\alpha \ or \ \beta)}{\pi}\right. \tag{14}$$

$$Twist[0, 90^\circ] = \frac{X}{L} \times 90^\circ \times twisted\ diraction \tag{15}$$

$$\beta = \left[\frac{\frac{LA_i}{\pi R^2 - LA_i}}{\frac{LA_{FD}}{\pi R^2 - LA_{FD}}}\right]^n \tag{16}$$

3. Experimental study

3.1. Experimental setup

The current study considered the impact of the four-lobe swirl generator and its transition parts, placed at the entrance of a circular stainless-steel tube, on thermal performance and flow field. Fig. 4 provides a photographic overview of the geometrical cross-section and details the experimental equipment utilized in this study. The four-lobed swirl device length is 200 mm, the twisted angle is 360°, and the equivalent diameter is 0.5 m. The lobed swirl device combined with two essential entry and exit transition parts at a length of 100 mm and their angle was gradually rotated from (45° to 90°) with an equivalent diameter of 0.5 m [25]. The entry section was extended enough to 800 mm in length to ensure the turbulent entrance flow at fully developed behaviour.

The test section is stainless steel with 800 mm length, 0.05 m diameter and 1 mm thickness. The test section was surrounded by an electrical helical coil connected to a multimeter and power regulator to ensure a constant heat flux. The electronic circuit of the heater was connected to a digital multimeter (BK PRECISION, 2831E), which was used to determine the voltage and current provided to the heater with a basic output power DC at a precision of 0.03 %. To recognize the rotational flow characteristics induced within the lobed swirl generator, measuring the surface temperature by inserting twelve thermocouples type K around the test section at three places (each place has four thermocouples) has been considered. Thermocouples (Type-K) as shown in Fig. 5 are considered to measure the temperature of fluid flow and the surface temperature of the test section. Three places along the tube test section to insert thermocouples have been adopted as seen in Fig. 5 (b). Four thermocouples were positioned in each place to investigate the characteristics of swirl flow. No thermocouples were immersed in the fluid to avoid the water being disturbed and to ensure an accurate result. To measure the fluid temperature, two calibrated thermocouples have been inserted at 1 mm depth at the inlet and the outlet of the system. The disturbance of the water at the inlet position is negligible due to the small depth of the thermocouple inserted and the existence of a fully developed turbulent flow. Each thermocouple used in the experiment has a uniform diameter of 0.5 mm. All thermocouples were securely fixed using OT-201-16-USA high-temperature conductive paste to ensure measurement accuracy. All

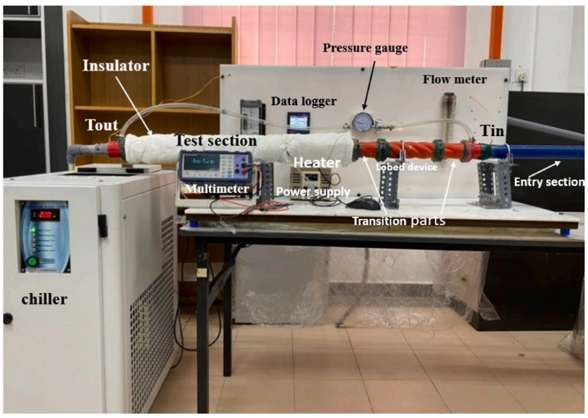

Fig. 4. Photo representation of the experimental setup.

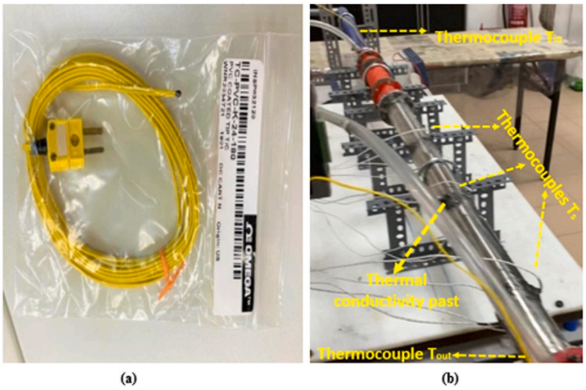

Fig. 5. a) Thermocouples type-K, b) Thermocouples distribution along the test section using high thermal conductive paste.

thermocouples are calibrated using a Temperature Calibrator Model (CL3512A). All thermocouples were connected with a data logger (SIMEX, CMC-99 MultiCon) to monitor the variation of the temperature change.

To avoid heat loss, the test tube is surrounded by a 1260 °C ceramic fibre blanket insulator. The experimental setup also contained a commercial water chiller (SPH20N) with a reservoir tank, temperature controller, water pump, and shut-off valves. The chiller offers a cooling capacity of 2400 kcal/h and ensures precise control of the working fluid temperature with an accuracy of ±0.2 °C. A flow meter (FCSD70-R50, TOFCO) with a ±0.5 % precision measurement range was installed at the inlet of the entry section to accurately measure the flow rate. A differential pressure gauge is mounted between two ends of the test section to determine the pressure difference over the channel. The average time value of all measurements and steady-state conditions are considered to assess the accuracy of observations. Once the reading of the measurements reached a steady state condition, the data were gathered. A steady state is achieved whenever the pressure and temperature measurements are stable for at least 5 min.

3.2. Preparation of hybrid nanofluid

Graphene oxide (GO) and Copper oxide (CuO) nanoparticles with average diameters of 3.9 nm and 40 nm, respectively, were used in the current experimental work. A scanning electron microscope (SEM) image of GO and CuO nanoparticles is depicted in Fig. 6. Due to the lower cost, production on a large scale, and dealing with oxide nanoparticles, a two-step method is adopted [52]. Pure water is utilized as the base fluid to synthesize the GO-CuO/water nanofluid.

The nanoparticles are weighed using a compassionate balance (Sartorius, M-pact AX224) with an accuracy of ±0.001 g. According to several volume concentrations form (0.15–0.75 %) using Eq. (17), the solid volume fraction was evaluated [53]. The hybrid nanoparticles were synthesized at different percentages, such as 80 % CuO and 20 % GO. A magnetic hotplate is employed to stir the water and nanoparticle mixtures for 1 h. To avoid the accumulation and sedimentation of hybrid nanoparticles, suspensions were treated for 10 h in a hot bath sonication (Benchtop Ultrasonic Cleaner SOO347181). The solid volume concentration measurement is listed in Table 2.

$$\varphi = \frac{\left(\frac{m}{\rho}\right)_{GO} + \left(\frac{m}{\rho}\right)_{CuO}}{\left(\frac{m}{\rho}\right)_{GO} + \left(\frac{m}{\rho}\right)_{CuO} + \left(\frac{m}{\rho}\right)_{Mixture}} \tag{17}$$

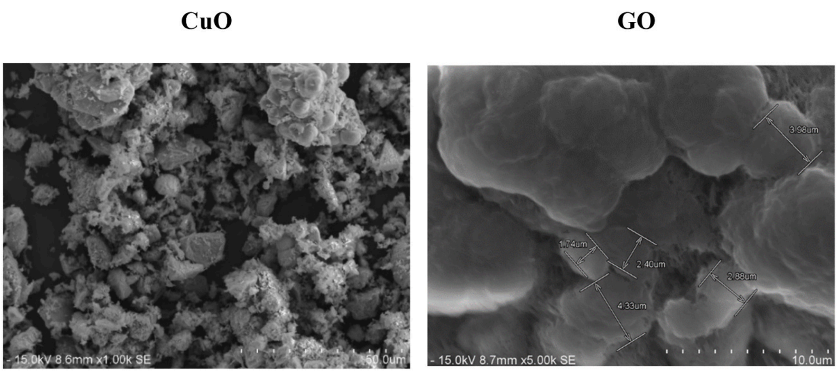

Fig. 6. SEM image of CuO and GO nanoparticles.

Table 2
The volume concentrations of nanoparticles used to make 100 ml of hybrid nanofluid.

Volume concentration (%)	Mass [±0.001] (g)	
	GO	CuO
0.15	0.03	0.757
0.30	0.06	1.517
0.45	0.09	2.278
0.60	0.121	3.042
0.75	0.151	3.809

where φ, m and ρ refer respectively to volume concentration, mass (kg) and density (kg/m^3)

3.3. Measuring thermophysical properties

At volume concentrations of 0.15, 0.30, 0.45, 0.60, and 0.75 %, the thermophysical properties of the GO-CuO/water hybrid nanofluid were experimentally measured. The density has been calculated based on the known volume and the mass of the hybrid nanofluid. The viscosity was measured using a Vibro viscometer (AND SV-100-Japan) of a range (0.3–10,000 mPa s) and an accuracy of 0.1 %. The KD2-pro device with an accuracy of 5 % W/m.K and a thermal conductivity ranging between 0.2 and 2 W/m.K was used to evaluate the thermal conductivity of the hybrid nanofluid. At the temperature range between −100 and +450, differential scanning calorimetry (DSC) was used to measure the specific heat. The average time value is considered to ensure the accuracy of the thermophysical properties measurement result. The hybrid nanofluid GO-CuO/water thermophysical properties obtained are illustrated in Table 3.

4. Data reduction

4.1. Data analysis approach

The entry section was extended enough to ensure the fully developed turbulent flow using the following formula [23]:

$$L_e = 4.4D \times (Re)^{1/6} \tag{18}$$

The constant heat flux generated by the electrical power via the plate heater can be calculated using the simplified steps as follows [19]:

$$Q_e = V \times I \tag{19}$$

The heat transfer generated by the working fluid is defined as [18]:

$$Q_f = \dot{m}C_p(T_{out} - T_{in}) \tag{20}$$

It can simply calculate the mass flow rate as a function of the Re, working fluid viscosity and the diameter of the geometrical cross-section using the following equation [54]:

$$\dot{m} = \frac{Re\mu\pi D}{4} \tag{21}$$

For more accuracy, Eq. (22) was used to determine the average value between the heat flux provided by electrical power (Q_e) and the heat transfer generated by the working fluid (Q_f) [9].

$$Q = \frac{Q_e + Q_f}{2} \tag{22}$$

The heat transfer between the test section and the internal flow is considered by convection. Therefore, the following equation was adopted to determine the convection heat transfer coefficient:

Table 3
Thermophysical properties measured of GO-CuO/water.

Properties	Water	GO-CuO/water 0.15 %	GO-CuO/water 0.30 %	GO-CuO/water 0.45 %	GO-CuO/water 0.60 %	GO-CuO/water 0.75 %
Density (kg/m^3)	997.31	1005.25	1010.75	1024.51	1038.27	1052.03
Viscosity (Pa.s)	0.001003	0.001016	0.001032	0.001043	0.001054	0.001068
Thermal conductivity (W/m.K)	0.66215	0.7074	0.7148	0.7193	0.7235	0.7264
Specific heat (J/kg K)	4182.61	4146.63	4123.37	4066.32	4010.76	3956.7

$$h_{ave} = \frac{Q}{\Delta T \times A_s} \tag{23}$$

$$\Delta T = T_w - T_b \tag{24}$$

Where T_w and T_b refer to the temperature of the wall and bulk temperature, respectively, the average temperature of the wall (T_w) and fluid (T_b) can be evaluated using Eqs. (24) and (25), respectively.

$$T_w = \frac{\textit{Sum of surface temperature observation}}{\textit{Total number of observation}} \tag{25}$$

$$T_b = \frac{T_{in} + T_{out}}{2} \tag{26}$$

$$Nu_{ave} = \frac{h_{ave} D_h}{k} \tag{27}$$

The friction factor can be obtained by measuring the pressure drop along the test section using the following formula [55]:

$$f = \frac{\Delta P}{(L/D)\left(\frac{\rho u_i^2}{2}\right)} \tag{28}$$

To investigate the applicability of the system in terms of thermal performance, Performance Evaluation Criteria (*PEC*) take place in this study using the following formula [9]:

$$PEC = \frac{Nu/Nu_p}{\left(f/f_p\right)^{1/3}} \tag{29}$$

Where *Nu* and Nu_p are the Nusselt numbers after enhancement and at the plane tube, respectively, while *f* and f_p are the friction factor after enhancement and at the plane tube, respectively.

4.2. Uncertainty analysis

To ensure the accuracy and reliability of the findings, the uncertainty analysis approach of all parameters used in the experimental study was considered. It is known that the uncertainty percentage of the parameters measured depends on the type of device used and the related equation of each variable. Consequently, the determination of the error utilizing the Kline and McClintock method was adopted [56]. Analyses are carried out to calculate the experimental uncertainties of the parameters that were obtained from the data reduction, such as Nusselt number (*Nu*), friction factor (*f*), and Reynolds number (*Re*) [52]. The differential approximation approach was considered to determine the uncertainty level in a result *Rs*, which is a function of the independent parameters *X1, X2, X3 …,* X_n. Therefore:

$$R = R(X_1, X_2, X_3, \ldots\ldots\ldots\ldots\ldots\ldots, X_n) \tag{30}$$

Where X_1, X_2, …. X_n and *R* are independent and dependent parameters. As a result, the following formula can be used to determine the uncertainty (*R*) [10]:

$$W_R = \pm\sqrt{\left(\frac{\partial R}{\partial X_1} W_{X_1}\right)^2 + \left(\frac{\partial R}{\partial X_2} W_{X_2}\right)^2 +, \ldots\ldots\ldots\ldots\ldots\ldots \left(\frac{\partial R}{\partial X_n} W_{X_n}\right)^2} \tag{31}$$

The maximum factor uncertainties were observed for (The Nusselt number, friction factor and Reynolds number using Eqs. (32)–(34) [57] respectively 5.6 %, 3.9 % and 6.3 %, while all the other parameters were found to be less than 5 %. Therefore, it is proved that the reliability of the experimental work presented a precision level acceptable for the instruments in use.

$$U_{Nu} = \pm\sqrt{\left(\frac{\partial Nu}{\partial q} U_q\right)^2 + \left(\frac{\partial Nu}{\partial D_h} U_{D_h}\right)^2 + \left(\frac{\partial Nu}{\partial K} W_K\right)^2} \tag{32}$$

$$U_f = \pm\sqrt{\left(\frac{\partial f}{\partial \Delta P} U_{\Delta P}\right)^2 + \left(\frac{\partial f}{\partial D_h} U_{D_h}\right)^2 + \left(\frac{\partial f}{\partial \rho} U_\rho\right)^2 + \left(\frac{\partial f}{\partial u_{ave}} U_{u_{ave}}\right)^2} \tag{33}$$

$$U_{Re} = \pm\sqrt{\left(\frac{\partial Re}{\partial \rho} U_\rho\right)^2 + \left(\frac{\partial Re}{\partial u} U_u\right)^2 + \left(\frac{\partial Re}{\partial D_h} U_{D_h}\right)^2 + \left(\frac{\partial Re}{\partial \mu} U_\mu\right)^2} \tag{34}$$

The absolute values are considered to attain the highest level of absolute uncertainty in the WR result since the number of values in the equation above and the errors in the measurement parameters can be positive and negative. Table 4 provides an overview and percentage of the range of uncertainty of *Re*, heat flux, heat transfer coefficient, *Nu*, and friction factor. In addition, all other parameters were found to be less than 5 %, proving that the experimental work's reliability presented a precision level acceptable for the instruments in use.

5. Results and discussion

5.1. Verification of experimental work

Correlations between the Nusselt number and the friction factor over the plane tube were carried out to assess the validity of the current experimental investigation [58]. In terms of Nusselt number, Dittus-Boelter Eq. (35) and Seider-Tate Eq. (36) were considered. As depicted in Fig. 7(a), there was a good agreement with a deviation of 3.63 % and 9.83 %, respectively, between the current experimental study and the correlations proposed by Dittus-Boelter and Seider-Tate. On the other hand, Fig. 7(b) demonstrates the reliability of the current experimental study in terms of the friction factor perspective.

The comparison between the present experimental approach and the correlations suggested by Brkic Eq. (37), Blasius Eq. (38) and Petukhov Eq. (39) [18] present a reliable result with acceptable precision of 2.46 %, 22.12 % and 24.12 %, respectively. Consequently, it can be proved that the experimental friction factor and heat transfer observations were reliable.

$$Nu = 0.023Re_b^{4/5}P_r^{0.4} \text{ where } P_r^{0.4} \text{ is for heating} \tag{35}$$

$$Nu = 0.027Re_b^{4/5}Pr_b^{1/3}\left(\frac{\mu}{\mu_s}\right)^{0.14} \tag{36}$$

Where the viscosity of the fluid at bulk temperature and the average wall temperature are written as μ and μ_s, respectively.

$$\frac{1}{\sqrt{f}} = -2\,log\left(\frac{\varepsilon}{3.71D} + \frac{2.18S}{Re_b}\right) \quad when$$

$$S = ln\left(\frac{Re}{1.816\frac{1.1Re}{\ln(1+1.1Re)}}\right) \tag{37}$$

$$f = 0.316Re_b^{-1/4} \tag{38}$$

$$f = (0.79\ln(Re_b) - 1.64)^{-2} \tag{39}$$

5.2. The performance of thermal conductivity

Developing highly efficient heat transfer fluids using nanofluids offers a cost-effective approach to minimizing heat loss, enhancing heat transfer efficiency, and accelerating cooling rates [59]. The thermal conductivity ratio and its enhancement relative to the base fluid are key factors in evaluating the performance of hybrid nanofluids. The thermal conductivity ratio is defined as the ratio of the thermal conductivity of the nanofluid (K_{nf}) to that of the base fluid (K_{bf}), expressed as K_{nf}/K_{bf}. The thermal conductivity ratio (TCR) and thermal conductivity enhancement (TCE) can be expressed mathematically as shown in Eqs. (40) and (41):

Table 4
Summary of uncertainty analysis.

Parameters	Value/Range	Uncertainty type	Uncertainty (%)
Nanoparticle weight (Sartorius)	Precision: 0.001 g	Absolute error	±0.001 g
Viscosity (AND SV-100)	0.3 to 10,000 mPa s	Relative error	±0.1 % of the reading
Thermal Conductivity	0.2–2 W/m. K	Relative error	±5 %
Specific Heat (DSC)	(-100 to +450 °C)	Relative error	±2 %
Voltage/Current to Heater	DC Output Power	Relative error	±0.03 % of the reading
Thermocouple Temperature	Various	Absolute error	±1.1 °C (above 100 °C)
Water Chiller Temperature	2 °C Accuracy	Absolute error	±0.2 °C
Differential Pressure	Pressure drop	Relative error	±0.5 %
Flow Rate (Tofco FC-SD85L-L200)	20-200 LPM	Relative error	±0.5 % FS
Reynolds number, *Re*	–	Derived	2.030 %
Heat flux, *q*	–	Derived	2.003 %
Heat transfer coefficient, *h*	–	Derived	0.232 %
Nusselt number, *Nu*	–	Derived	7.787 %
Friction factor, *f*	–	Derived	2.441 %

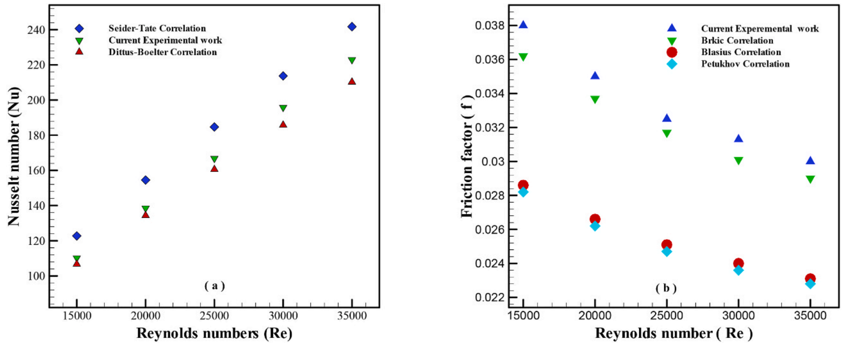

Fig. 7. Verification of current experimental work versus different correlation over plane tube (a) Nusselt number (b) Friction factor.

$$Thermal\ conductivivty = \frac{K_{nf}}{K_{bf}} \tag{40}$$

$$Thermal\ conductivity\ enhancement\ (\%) = \frac{K_{nf} - K_{bf}}{K_{bf}} \tag{41}$$

The **thermal conductivity ratio (TCR)** is analyzed across different **volume concentrations** and **temperatures** to evaluate its variation and influence on heat transfer performance. Fig. 8(a) illustrates the variation of the thermal conductivity ratio (TCR) as a function of the solid volume fraction, highlighting the impact of different temperatures on thermal conductivity enhancement. In contrast, Fig. 8(b) depicts the thermal conductivity ratio (TCR) as a function of temperature, evaluated at different nanoparticle volume concentrations. The results revealed varying slope trends with a generally consistent increase in the thermal conductivity ratio (TCR) across different conditions. The TCR increased from 1.062 at 25 °C with a 0.15 % volume concentration to 1.097 at 50 °C with a 0.75 % volume concentration, confirming the influence of nanoparticle volume fraction and temperature on enhancing relative thermal conductivity. The findings demonstrated that TCR increased with the addition of solid volume fraction and the selected temperature range. However, no consistent slope pattern was observed for different mass fractions and temperatures. For instance, for the GO-CuO/water hybrid nanofluid at 0.15 % volume concentration, TCR increased from 1.0625 at 25 °C to 1.07 at 50 °C, representing a 0.943 % improvement. Similarly, for the 0.75 % volume fraction, TCR increased from 1.081 at 25 °C to 1.0965 at 50 °C, reflecting a 1.53 % improvement. This enhancement in TCR can be attributed to the increased nanoparticle interactions due to higher suspension levels and elevated temperatures, leading to a rise in the surface-to-volume ratio and improved heat transfer characteristics. According to the thermal conductivity enhancement (TCE) results, as illustrated in Fig. 9, the findings highlight the influence of temperature and nanoparticle volume concentration on improving thermal conductivity. The results indicate that higher temperatures and volume concentrations contribute to greater enhancement. The maximum thermal conductivity enhancement of 8.8 % was observed at 50 °C with a 0.75 % volume concentration, demonstrating the significant impact of these parameters on the thermal performance of the hybrid nanofluid.

5.3. Heat transfer

5.3.1. Compression between the lobed swirl and plan tube

Fig. 10 depicted a comparison between a lobed swirl generator and a plain tube under water as working fluid. The result revealed

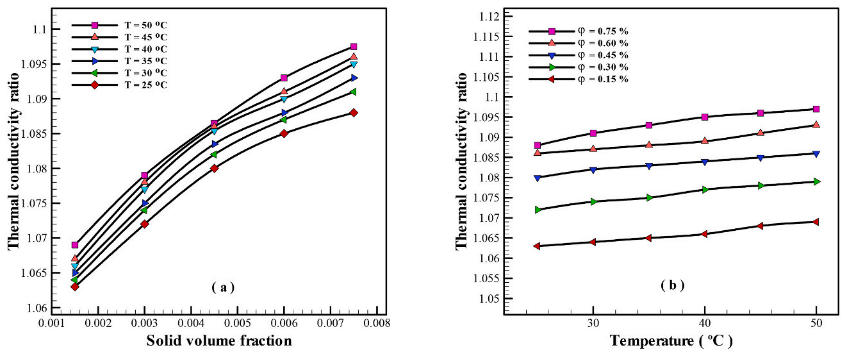

Fig. 8. Experimental study of the variation of thermal conductivity ratio by (a) a different temperature at the impact of solid volume fraction and (b) a different solid volume fraction at the impact of temperature.

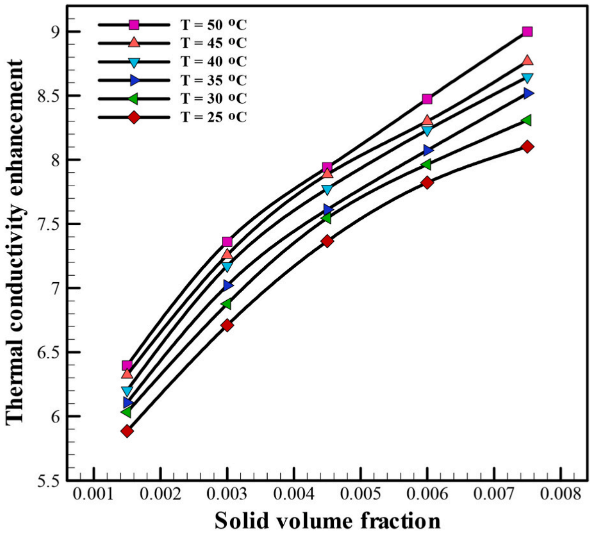

Fig. 9. Experimental study of the variation of thermal conductivity enhancement by a different volume concentration at various temperatures.

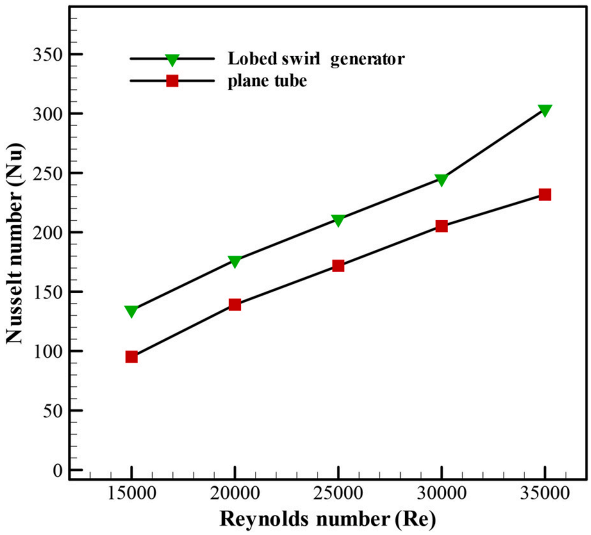

Fig. 10. Heat transfer characteristics at the impact of lobed swirl and plane tube using water as working fluid.

that the lobed swirl generator presented a significant advantage in heat transfer enhancement due to its ability to induce swirl flow, increase turbulence, and disrupt thermal boundary layers, leading to higher Nusselt numbers and better heat transfer efficiency. On the other hand, the plain tube offers a lower pressure drop and simpler design but lacks the necessary turbulence generation for effective heat transfer enhancement, particularly at lower Reynolds numbers. Therefore, the choice between these two configurations depends on the specific application requirements, balancing thermal performance, energy efficiency, and operational constraints.

5.3.2. Heat transfer of lobed swirl generator using GO/CuO hybrid nanofluid under different volume concentration

The main target of the current experimental study is to examine the thermal performance of lobe swirl generators under different working fluids (water & Graphene-CuO/water nanohybrid). It is expected that the benefit lobe swirl generator of induced tangential velocity near the wall and enhanced thermal conductivity of working fluid by adding a hybrid nanofluid will have considerably increased thermal performance. The effect of the lobe swirl generator at different working fluids under the variations of nanoparticle volume concentration and *Re* on heat transfer enhancement is shown in Fig. 11. The optimal parameters for the lobed swirl generator were a twisted angle of the twisted angle of ($\theta = 360^\circ$), twisted length of ($l = 0.4$ m), beta transition at a transition multiplier of ($n = 0.25$ mm), and variable helix of ($t = 1$) [20]. The impact of the concentration of hybrid nanofluid volume fraction on heat transfer was observed at all amounts of volume fraction adopted. In other words, the increase in nanoparticle volume concentration led to an increase in Nusselt number due to the proportional relationship between the amount of volume fraction and thermal conductivity.

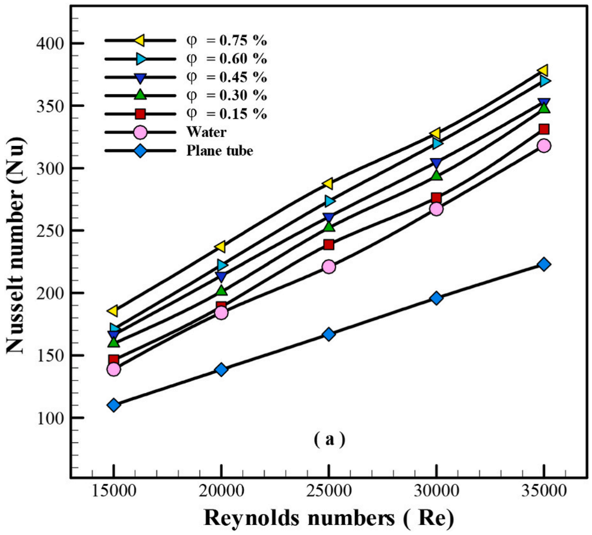

Fig. 11. Effect of lobe swirl generator under different volume concentrations and *Re* on heat transfer.

Additionally, the feature of lobed swirl generators to keep the nanoparticles in suspension [51] and the stirring character of a high Reynolds number have a considerable impact on avoiding the agglomeration of nanoparticles, which helps prevent pipeline blockage. Fig. 12 demonstrates the characteristics of the value of the Nusselt number versus different Reynolds numbers at the variation of hybrid nanoparticle volume fractions. The outcome exhibited a 1.76-factor increase in heat transfer value at a *Re* of 25,000. It can be explained by the feature of the lobed swirl generator, which is represented by its ability to distribute the particles of the working fluid at low flow velocity [51]. In general, the result demonstrates the capability of a lobe swirl generator to improve heat transfer under various factors.

5.4. Friction factor

The average temperature between the input and output is considered to assess all thermal flow properties [55]. To evaluate the friction factor of the nanohybrids over the test section, Eq. (28) is used. Fig. 13 illustrates the friction factor that occurs by the lobe swirl generator under the variation of working fluids (water & hybrid nanofluids), nanoparticles volume fraction and *Re*. The overall trend shows that the friction factor decreases with an increase in *Re* and vice versa. Additionally, the friction factor gradually increases as the nanoparticle volume concentration increases, which can be explained by the perturbation (disturbance), flow blockage caused by the added hybrid nanoparticles, the centrifugal force of the lobe swirl, and turbulent flow fluctuations. The ratio between the friction factor at different volume concentrations and the friction factor at the plane tube is illustrated in Fig. 14. The result indicated that the maximum difference in friction factor value is 1.53, which is associated with high volume fraction and *Re*. The result revealed a proportional relationship between the friction factor and the increase of nanoparticle volume fraction and high Reynolds number.

5.5. Performance evaluation criteria

To evaluate the Performance Evaluation Criterion (PEC), Eq. (29) has been adopted, which is typically used to quantify the trade-off between heat transfer enhancement and the associated pressure loss. The PEC provides a comprehensive measure of thermal performance, enabling comparison of different heat exchanger configurations or fluid combinations. According to the experimental data implied in A **performance evaluation criterion (PEC) greater than one** indicates that the enhancement in heat transfer surpasses the impact of the friction factor, as observed in previous studies [52]. The result revealed that the highest values of PEC recorded at the *Re* of 25,000 are 1.309, 1.372, 1.41, 1.457 and 1.511 at a volume concentration of 0.15 %, 30 %, 0.45 %, 0.60 % and 0.75 % respectively as shown in Fig. 15. Therefore, the improvement in this value of the *Re* can be attributable to the dramatic augmentation of the friction factor at a high *Re* together with the curvature surface of the lobe swirl generator cross-section. On the other hand, the enhancement of the thermal conductivity of hybrid nanoparticles at high concentrations led to overcoming the pressure drop penalty by improving the heat transfer. The lobed swirl generator in this study offers a distinctive mechanism that enhances heat transfer, stabilizes particle suspension, and optimizes pressure loss, positioning it as a viable solution for advanced thermal control systems. These combined features make it a compelling alternative for various applications, especially in sectors where efficient heat exchange and precise fluid flow management are critical to overall system performance. The lobe swirl generator plays a crucial role in enhancing thermal performance and optimizing fluid flow characteristics. Its primary functions include; (i) increasing swirl intensity, leading to improved fluid mixing and heat transfer enhancement [50]. (ii) Due to its advantage of transition parts (entry and exit) [51], it helps sustain the uniform dispersion of GO/CuO hybrid nanofluid particles, reducing particle settling. This ensures consistent thermal conductivity and

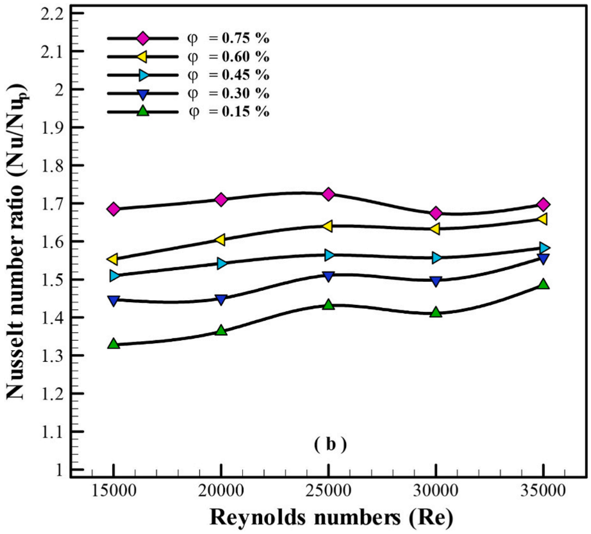

Fig. 12. Effect of lobe swirl generator under different volume concentrations and *Re* on heat transfer ratio.

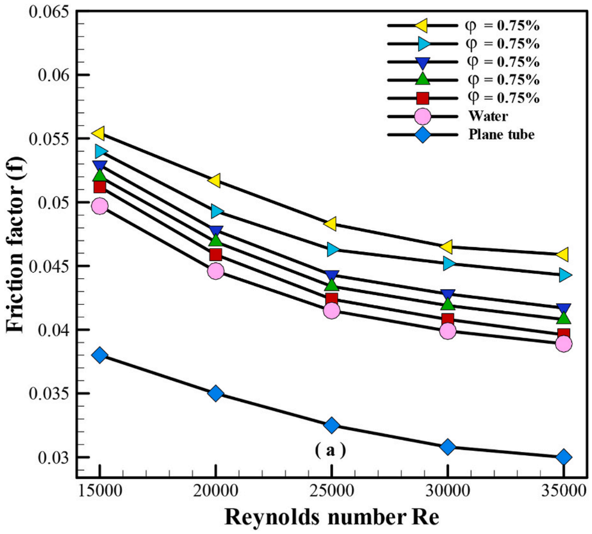

Fig. 13. Effect of lobe swirl generator under different volume concentrations and *Re* on friction factor.

prevents sedimentation [60], which is a common challenge in nanofluid applications. (iii) Unlike conventional swirl generators that cause excessive pressure drops, the lobed design balances swirl generation and pressure loss, making it more efficient for practical applications. This study presents a novel investigation into the thermal performance of a lobed swirl generator in conjunction with a GO-CuO/water hybrid nanofluid, addressing critical gaps in heat transfer enhancement techniques. Unlike conventional swirl flow devices, the four-lobed swirl generator introduces enhanced flow mixing and turbulence, significantly improving heat transfer efficiency while maintaining an acceptable pressure loss. This phenomenon can be attributed to the increase in **tangential velocity** resulting from a decrease in the **multiplier (*n*),** as demonstrated by **Ariyaratne** [51]. A high-**performance evaluation criterion (PEC)** value signifies an enhanced heat transfer rate, as observed in the **study** [61]. The result also presented a polynomial relation between a PEC and a given value of Reynolds number. The outcome is also highly consistent with the result given by Jafari et al. [10].

A key innovation lies in the synthesis and application of the GO-CuO/water nanohybrid at varying volume concentrations (0.15%–0.75 % wt.), presenting a unique combination of graphene oxide (GO) and copper oxide (CuO) nanoparticles to optimize thermal conductivity and viscosity. The experimental findings demonstrate a notable heat transfer enhancement of up to 1.76, with the highest thermal performance factor of 1.51 observed at a high nanoparticle concentration (0.75 %) and a moderate Reynolds number ($Re =$ 25,000). This study provides new insights into the interplay between swirl-induced turbulence, hybrid nanofluid thermophysical properties, and flow dynamics, contributing to the advancement of next-generation heat exchanger technologies. The findings hold significant implications for energy-efficient thermal management systems, including applications in HVAC, automotive cooling, and

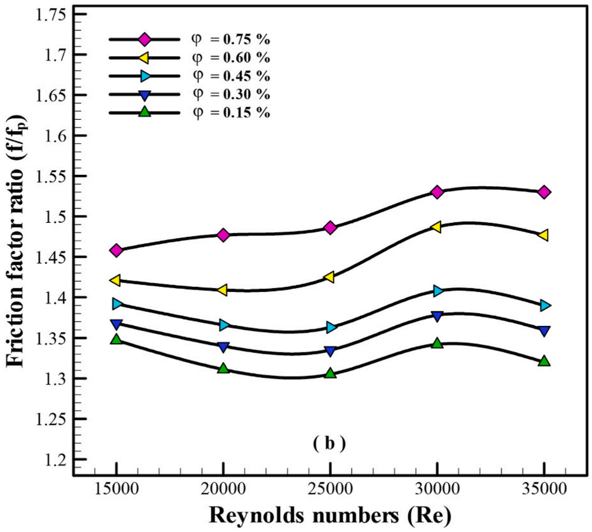

Fig. 14. Effect of lobe swirl generator under different volume concentrations and *Re* on friction factor ratio.

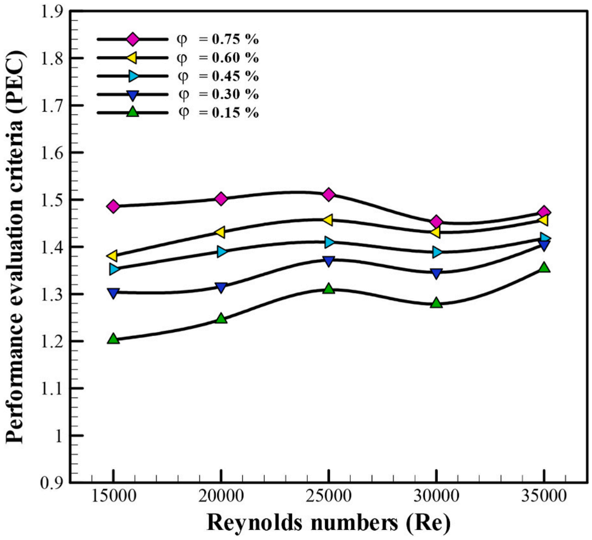

Fig. 15. Effect of lobe swirl generator under different volume concentrations and *Re* on thermal performance.

industrial heat exchangers.

6. Conclusion

This study investigated the thermal performance of a lobed swirl generator using GO-CuO/water hybrid nanofluid at varying volume concentrations (0.15 %–0.75 %) and Reynolds numbers (15,000 to 35,000). The employed geometry consists of two primary sections: (1) a lobed swirl device with a length of 200 mm, a twist angle of 360°, and a pitch-to-diameter ratio of 8 as key influencing parameters, and (2) a transition section with a length of 100 mm, which gradually transforms from a circular to a lobed cross-section between angles of 45° to 90° and vice versa. All the physical properties of the hybrid nanofluid are experimentally measured. The experimental results demonstrated that the lobed swirl generator significantly enhanced heat transfer from 1.26 to 1.72, with a slight increment in friction factor between 1.27 and 1.53. The Performance Evaluation Criterion (PEC) of 1.51 at an optimal volume concentration of 0.75 % and a Reynolds number of 25,000 has been obtained. The findings highlight the potential of the lobed swirl generator to improve heat exchanger efficiency while maintaining an acceptable pressure drop. Despite these promising results, further research is required to optimize the design parameters and assess long-term stability. Future studies could explore the impact of different swirl geometries, nanofluid compositions, and operating conditions to maximize thermal performance. Additionally, numerical simulations combined with experimental validation can provide deeper insights into the underlying flow dynamics and heat transfer mechanisms. Expanding this research to include higher Reynolds numbers and varying working fluids would further establish the effectiveness of lobed swirl generators in real-world thermal applications such as HVAC systems, automotive cooling, and industrial heat exchangers.

CRediT authorship contribution statement

Farag A. Diabis: Writing – original draft, Visualization, Validation, Methodology, Investigation, Formal analysis, Data curation, Conceptualization. **Abd Rahim Abu Talib:** Writing – review & editing, Supervision, Resources, Project administration, Funding acquisition. **Norkhairunnisa Mazlan:** Supervision. **Eris Elianddy Supeni:** Supervision.

Declaration of competing interest

The authors declare that they have no known competing financial interests or personal relationships that could have appeared to influence the work reported in this paper.

Acknowledgements

The research was funded under the MySIP grant scheme no. 5540547 from Ministry of Higher Education Malaysia.

Data availability

Data will be made available on request.

References

[1] K. Azeez, A.R.A. Talib, R.I. Ahmed, Heat transfer enhancement for corrugated facing step channels using aluminium nitride nanofluid - numerical investigation, J. Therm. Eng. 8 (6) (2022) 734–747, https://doi.org/10.18186/thermal.1197106.
[2] I. Carrillo-Berdugo, et al., Improving the efficiency of the concentrating solar power plants using heat transfer nanofluids with gold nanoplates: an analysis from laboratory to industrial scale, J. Mol. Liq. 376 (2023), https://doi.org/10.1016/j.molliq.2023.121415.
[3] Y.L. Liu, C. Zhang, S.Y. Li, Z.M. Li, Study of steam heat transfer enhanced by CO2 and chemical agents: in heavy oil production, Pet. Sci. 20 (2) (2022) 1030–1043, https://doi.org/10.1016/j.petsci.2022.09.034.
[4] A.R. Abu Talib, A.K. Hilo, Fluid flow and heat transfer over corrugated backward facing step channel, Case Stud. Therm. Eng. 24 (December 2020) (2021) 100862, https://doi.org/10.1016/j.csite.2021.100862.
[5] J. Chen, J. Zhou, X. Li, X. Huai, Study of the heat transfer characteristics and waste heat recovery of hot gas with coagulative particles flowing through a moving granular bed filter (MGBF), Appl. Therm. Eng. 211 (August 2021) 118444, https://doi.org/10.1016/j.applthermaleng.2022.118444, 2022.
[6] A. Elghool, et al., Enhancing the performance of a thermo-electric generator through multi-objective optimisation of heat pipes-heat sink under natural convection, Energy Convers. Manag. 209 (November 2019) (2020) 112626, https://doi.org/10.1016/j.enconman.2020.112626.
[7] A.R.A. Talib, S. Salman, M.F.M. Zulkeple, A.K. Hilo, Experimental investigation of nanofluid turbulent flow over microscale backward-facing step, J. Adv. Res. Fluid Mech. Therm. Sci. 99 (2) (2022) 119–134, https://doi.org/10.37934/arfmts.99.2.119134.
[8] K. Sefiane, A. Koşar, Prospects of heat transfer approaches to dissipate high heat fluxes: opportunities and challenges, Appl. Therm. Eng. 215 (February) (2022), https://doi.org/10.1016/j.applthermaleng.2022.118990.
[9] X. Tang, X. Dai, D. Zhu, Experimental and numerical investigation of convective heat transfer and fluid flow in twisted spiral tube, Int. J. Heat Mass Tran. 90 (2015) 523–541, https://doi.org/10.1016/j.ijheatmasstransfer.2015.06.068.
[10] M. Jafari, M. Farhadi, K. Sedighi, Thermal performance enhancement in a heat exchanging tube via a four-lobe swirl generator : an experimental and numerical approach, Appl. Therm. Eng. 124 (2017) 883–896, https://doi.org/10.1016/j.applthermaleng.2017.06.095.
[11] E.U. Gorelikov, I.V. Naumov, M.A. Tsoy, V.N. Shtern, Heat transfer in a centrifugal vortex tube, J. Phys. Conf. Ser. 2119 (1) (2021), https://doi.org/10.1088/1742-6596/2119/1/012065.
[12] M. Sheikholeslami, M. Gorji-Bandpy, D.D. Ganji, Review of heat transfer enhancement methods: focus on passive methods using swirl flow devices, Renew. Sustain. Energy Rev. 49 (2015) 444–469, https://doi.org/10.1016/j.rser.2015.04.113.
[13] A.A.R. Al Kumait, T.K. Ibrahim, M.A. Abdullah, Experimental and numerical study of forced convection heat transfer in different internally ribbed tubes configuration using TiO2 nanofluid, Heat Tran. Asian Res. 48 (5) (2019) 1778–1804, https://doi.org/10.1002/htj.21457.
[14] T.K. Ibrahim, et al., Experimental study on the effect of perforations shapes on vertical heated fins performance under forced convection heat transfer, Int. J. Heat Mass Tran. 118 (3 November) (2018) 832–846, https://doi.org/10.1016/j.ijheatmasstransfer.2017.11.047.
[15] T.K. Ibrahim, A.T. Al-Sammarraie, M.S.M. Al-Jethelah, W.H. Al-Doori, M.R. Salimpour, H. Tao, The impact of square shape perforations on the enhanced heat transfer from fins: experimental and numerical study, Int. J. Therm. Sci. 149 (March 2019) (2020) 106144, https://doi.org/10.1016/j.ijthermalsci.2019.106144.
[16] M. Omidi, M. Farhadi, Numerical study on the effect of using spiral tube with lobed cross section in double-pipe heat exchangers, J. Therm. Anal. Calorim. 123456789 (3) (2018) 2397–2408, https://doi.org/10.1007/s10973-018-7579-y.
[17] H.E. Ahmed, M.I. Ahmed, M.Z. Yusoff, M.N.A. Hawlader, H. Al-Ani, Experimental study of heat transfer augmentation in non-circular duct using combined nanofluids and vortex generator, Int. J. Heat Mass Tran. 90 (2015) 1197–1206, https://doi.org/10.1016/j.ijheatmasstransfer.2015.07.065.
[18] M. Jafari, S. Dabiri, M. Farhadi, K. Sedighi, Effects of a three-lobe swirl generator on the thermal and flow fields in a heat exchanging tube: an experimental and numerical approach, Energy Convers. Manag. 148 (2017) 1358–1371, https://doi.org/10.1016/j.enconman.2017.06.074.
[19] M. Jafari, M. Farhadi, K. Sedighi, An experimental study on the effects of a new swirl generator on thermal performance of a circular tube, Int. Commun. Heat Mass Tran. 87 (August) (2017) 277–287, https://doi.org/10.1016/j.icheatmasstransfer.2017.07.016.
[20] F.A. Diabis, A. Rahim, A. Talib, Y. Al-tarazi, N. Mazlan, E. Elianddy, Thermal performance of four-lobe swirl generator and its transition parts under a different type of nanofluids, CFD Lett. 11 (11) (2022) 63–74, https://doi.org/10.37934/cfdl.14.11.6374.
[21] B. Indurain, D. Uystepruyst, F. Beaubert, S. Lalot, Helgadóttir, Numerical investigation of several twisted tubes with non-conventional tube cross sections on heat transfer and pressure drop, J. Therm. Anal. Calorim. 140 (3) (2020) 1555–1568, https://doi.org/10.1007/s10973-019-08965-4.
[22] M. Omidi, A.A. Rabienataj, D. Mousa, A.A. Rabienataj Darzi, M. Farhadi, Turbulent heat transfer and fluid flow of alumina nanofluid inside three-lobed twisted tube, J. Therm. Anal. Calorim. 137 (4) (2019) 1451–1462, https://doi.org/10.1007/s10973-019-08026-w.
[23] T. Yan, J. Qu, X. Sun, Y. Chen, Q. Hu, W. Li, Numerical evaluation on the decaying swirling flow in a multi-lobed swirl generator, Eng. Appl. Comput. Fluid Mech. 14 (1) (2020) 1198–1214, https://doi.org/10.1080/19942060.2020.1816494.

[24] G. Li, P. Hall, N. Miles, T. Wu, Optimization of a four-lobed swirl pipe for Clean-In-Place procedures, International Journal of Environmental 9 (6) (2015) 689–697, https://doi.org/10.13140/RG.2.1.4838.0004.

[25] T. Ariyaratne, C and Jones, Design and optimization of swirl pipe geometry for particle-laden liquids, AIChE J. 59 (4) (2007) 757–768, https://doi.org/10.1002/aic.

[26] M. Gupta, V. Singh, Z. Said, Heat transfer analysis using zinc Ferrite/water (Hybrid) nanofluids in a circular tube: an experimental investigation and development of new correlations for thermophysical and heat transfer properties, Sustain. Energy Technol. Assessments 39 (January) (2020) 100720, https://doi.org/10.1016/j.seta.2020.100720.

[27] H. Babar, H.M. Ali, Towards hybrid nanofluids: preparation, thermophysical properties, applications, and challenges, J. Mol. Liq. 281 (2019) 598–633, https://doi.org/10.1016/j.molliq.2019.02.102.

[28] I.A. Zakaria, W.A.N.W. Mohamed, N.H.A. Azid, M.A. Suhaimi, W.H. Azmi, Heat transfer and electrical discharge of hybrid nanofluid coolants in a fuel cell cooling channel application, Appl. Therm. Eng. 210 (August 2021) (2022) 118369, https://doi.org/10.1016/j.applthermaleng.2022.118369.

[29] T. Salahuddin, N. Siddique, M. Khan, Y.M. Chu, A hybrid nanofluid flow near a highly magnetized heated wavy cylinder, Alex. Eng. J. 61 (2) (2022) 1297–1308, https://doi.org/10.1016/j.aej.2021.06.014.

[30] H. Pandey, N. Kumar Gupta, A descriptive review of the thermal transport mechanisms in mono and hybrid nanofluid-filled heat pipes and current developments, Therm. Sci. Eng. Prog. 31 (March) (2022) 101281, https://doi.org/10.1016/j.tsep.2022.101281.

[31] Q. Xiong, et al., A comprehensive review on the application of hybrid nanofluids in solar energy collectors, Sustain. Energy Technol. Assessments 47 (June) (2021), https://doi.org/10.1016/j.seta.2021.101341.

[32] P. Kumar Kanti, P. Sharma, K.V. Sharma, M.P. Maiya, The effect of pH on stability and thermal performance of graphene oxide and copper oxide hybrid nanofluids for heat transfer applications: application of novel machine learning technique, J. Energy Chem. 82 (April) (2023) 359–374, https://doi.org/10.1016/j.jechem.2023.04.001.

[33] R. Taherialekouhi, S. Rasouli, A. Khosravi, An experimental study on stability and thermal conductivity of water-graphene oxide/aluminum oxide nanoparticles as a cooling hybrid nanoflui, Int. J. Heat Mass Tran. 145 (16-September) (2019) 118751, https://doi.org/10.1016/j.ijheatmasstransfer.2019.118751.

[34] S. Rostami, A.A. Nadooshan, A. Raisi, An experimental study on the thermal conductivity of new antifreeze containing copper oxide and graphene oxide nano-additives, Powder Technol. 345 (October) (2019) 658–667, https://doi.org/10.1016/j.powtec.2019.01.055.

[35] P.K. Kanti, V. Vicki Wanatasanappan, N. Mahjoub Said, K.V. Sharma, Stability, thermophysical properties, forced convective heat transfer, entropy minimization and exergy performance of a novel hybrid nanofluid: experimental study, J. Mol. Liq. 410 (July) (2024) 125571, https://doi.org/10.1016/j.molliq.2024.125571.

[36] I.P. Moghadam, M. Afrand, B. Mahmoudi, A.A. Barzinjy, P. Talebizadehsardari, Curve-fitting on experimental data for predicting the thermal-conductivity of a new generated hybrid nanofluid of graphene oxide-titanium oxide/water, Phys. A Stat. Mech. its Appl. 548 (April) (2019) 122–140, https://doi.org/10.1016/j.physa.2019.122140.

[37] J. Singh, R. Kumar, M. Gupta, H. Kumar, Thermal conductivity analysis of GO-CuO/DW hybrid nanofluid, Mater. Today Proc. 28 (May-2020) (2020) 1714–1718, https://doi.org/10.1016/j.matpr.2020.05.134.

[38] E. Roohani, D. Toghraie, Heat transfer improvement of antifreeze by changing it to hybrid nanofluid: effects of hybrid magnesium oxide–graphene oxide nanopowders, J. Therm. Anal. Calorim. (2021) 0123456789, https://doi.org/10.1007/s10973-021-10973-2, 1–15.

[39] P.K. Kanti, V.V. Wanatasanappan, P. Sharma, N.M. Said, K.V. Sharma, Experimental and machine learning insights on heat transfer and friction factor analysis of novel hybrid nanofluids subjected to constant heat flux at various mixture ratios, Int. J. Therm. Sci. 209 (August 2024) (2025) 109548, https://doi.org/10.1016/j.ijthermalsci.2024.109548.

[40] I. Kazemi, M. Sefid, M. Afrand, Improving the thermal conductivity of water by adding mono & hybrid nano-additives containing graphene and silica: a comparative experimental study, Int. Commun. Heat Mass Tran. 116 (2020) 104648, https://doi.org/10.1016/j.icheatmasstransfer.2020.104648.

[41] D. Li, Y. Wang, M. Guo, M. Song, Y. Ren, Preparation and thermophysical properties of graphene oxide–silver hybrid nanofluids, Bull. Mater. Sci. 43 (1) (2020) 1–6, https://doi.org/10.1007/s12034-020-02146-y.

[42] R. Bakhtiari, B. Kamkari, M. Afrand, A. Abdollahi, Preparation of stable TiO2-Graphene/Water hybrid nanofluids and development of a new correlation for thermal conductivity, Powder Technol. 385 (5 March) (2021) 466–477, https://doi.org/10.1016/j.powtec.2021.03.010.

[43] P.K. Kanti, P. Sharma, M.P. Maiya, K.V. Sharma, The stability and thermophysical properties of Al2O3-graphene oxide hybrid nanofluids for solar energy applications: application of robust autoregressive modern machine learning technique, Sol. Energy Mater. Sol. Cells 253 (January) (2023) 112207, https://doi.org/10.1016/j.solmat.2023.112207.

[44] S. Tian, N. Izza, D. Toghraie, S.A. Eftekhari, Using perceptron feed-forward Artificial Neural Network (ANN) for predicting the thermal conductivity of graphene oxide-Al2O3/water-ethylene glycol hybrid nanofluid, Case Stud. Therm. Eng. 26 (April) (2021) 101055, https://doi.org/10.1016/j.csite.2021.101055.

[45] S. Veeramachaneni, S.K. Pisipaty, D.R. Vedula, A.B. Solomon, V.S. Harsha, Effect of copper–graphene hybrid nanoplatelets in a miniature loop heat pipe, J. Therm. Anal. Calorim. 147 (10) (2021) 5985–5999, https://doi.org/10.1007/s10973-021-10873-5.

[46] M.R.H. Alhakeem, Enhancing thermal conductivity and heat transfer using graphene nanofluid, Int. J. Multidiscip. Sci. Arts 1 (1) (2022) 95–103, https://doi.org/10.47709/ijmdsa.v1i1.1710.

[47] Y. Guangbin, et al., Experimental research on heat transfer characteristics of CuO nanofluid in adiabatic condition, J. Nanomater. 2016 (1) (2016) 3693249, https://doi.org/10.1155/2016/3693249.

[48] D.W. Baker, C.L. Sayre, Decay of swirling turbulent flow of incompressible fluids in long pipes, in: H.W. Stoll (Ed.), Flow its Meas. Control Sci. Ind. Proc. ASME Fluids Eng. Conf. Vol. 1. Instrum. Soc, Am, Pittsburgh, 1974, pp. 301–312.

[49] Guozhen Li, Investigation of Swirl Pipe for Improving Cleaning Efficiency in Closed Processing System, University of Nottingham, 2016. PhD Thesis.

[50] G. Li, P. Hall, N. Miles, T. Wu, Improving the efficiency of 'Clean-In-Place' procedures using a four-lobed swirl pipe: a numerical investigation, Comput. Fluids 108 (2015) 116–128, https://doi.org/10.1016/j.compfluid.2014.11.032.

[51] C. Ariyaratne, T.F. Jones, Design and optimization of swirl pipe geometry for particle-laden liquids, AIChE J. 53 (4) (Apr. 2007) 757–768, https://doi.org/10.1002/aic.11122.

[52] A.K. Hilo, A.R.A. Talib, A.A. Iborra, M.T.H. Sultan, M.F.A. Hamid, Experimental study of nanofluids flow and heat transfer over a backward-facing step channel, Powder Technol. 372 (2020) 497–505, https://doi.org/10.1016/j.powtec.2020.06.013.

[53] S.R. Nfawa, A.R. Abu Talib, A.A. Basri, S.U. Masuri, Novel use of MgO nanoparticle additive for enhancing the thermal conductivity of CuO/water nanofluid, Case Stud. Therm. Eng. 27 (2021) 101279, https://doi.org/10.1016/j.csite.2021.101279.

[54] S.R. Chaurasia, R.M. Sarviya, Experimental thermal performance analysis of fluid flow in a heat exchanger pipe with novel double strip helical screw tape inserts for utilization of energy resources, Energy Sources, Part A Recover. Util. Environ. Eff. 00 (2-July) (2019) 1–14, https://doi.org/10.1080/15567036.2019.1669741.

[55] A.K. Hilo, A.R.A. Talib, A.A. Iborra, M.T.H. Sultan, M.F.A. Hamid, Experimental study of nanofluids flow and heat transfer over a backward-facing step channel, Powder Technol. 372 (2020) 497–505, https://doi.org/10.1016/j.powtec.2020.06.013.

[56] S. Kline, F. McClintock, Describing uncertainties in single-sample experiments, Mech. Eng. 75 (1953) 3–8.

[57] A.R. Abu Talib, S. Salman, Heat transfer and fluid flow analysis over the microscale backward-facing step using βGa_2O_3 nanoparticles, Exp. Heat Transf. 00 (00) (2022) 1–18, https://doi.org/10.1080/08916152.2022.2039328.

[58] S. Liu, M. Sakr, A comprehensive review on passive heat transfer enhancements in pipe exchangers, Renew. Sustain. Energy Rev. 19 (2013) 64–81, https://doi.org/10.1016/j.rser.2012.11.021.

[59] M. Pavia, K. Alajami, P. Estellé, A. Desforges, B. Vigolo, A critical review on thermal conductivity enhancement of graphene-based nanofluids, Adv. Colloid Interface Sci. 294 (2021) 102452.
[60] R.A.A. Raja, J. Sunil, R. Maheswaran, Estimation of thermo-physical properties of nanofluids using theoretical correlations, Int. J. Appl. Eng. Res. 13 (10) (2018) 7950–7953.
[61] S.R. Nfawa, A.R.A. Talib, S.U. Masuri, A.A. Basri, H. Hasini, Heat transfer enhancement in a corrugated-trapezoidal channel using winglet vortex generators, CFD Lett. 11 (10) (2019) 69–80.